http://www.jctjournals.com ISSN(ONLINE):2278 – 3814

Volume-15, Issue-06, June 2026
JOURNAL OF COMPUTING TECHNOLOGIES (JCT)
International Journal
Page Number: 01-09

Performance Evaluation of Refrigerants R-134a, and R-409A Based on Condensation Heat Transfer Correlations for Refrigeration Applications

Mohd Zaid[1], Prof. Amit Asthna[2]
[1]M.Tech Scholar, [2]Assistant Professor,
[1,2]Department of Mechanical Engineering *(ME)*
[1,2] Truba Institute of Engg. & Information Technology (*TIEIT*), Bhopal, INDIA

Abstract*—This study presents a comprehensive comparative evaluation of the condensation heat transfer characteristics of refrigerants r-12, r-134a, and r-409a using six widely accepted condensation heat transfer correlations: shah, cavallini and zecchin, bohdal, traviss, huang, and park. The analysis was conducted for a horizontal smooth tube with an internal diameter of 8 mm, an external diameter of 9.52 mm, and a length of 5 m under a constant condensing temperature of 45°c, mass flux ranging from 25 to 450 kg•m⁻²•s⁻¹, and vapor quality varying from 0 to 1. The objective was to investigate the influence of refrigerant thermophysical properties on condensation heat transfer behavior and to assess the predictive capability of different condensation heat transfer correlations. The results indicate that the average condensation heat transfer coefficient increases with increasing mass flux for all refrigerants due to enhanced convective condensation and reduced condensate film thickness. The bohdal correlation predicted the highest heat transfer coefficients for r-409a, whereas the shah, cavallini and zecchin, traviss, huang, and park correlations consistently identified r-134a as exhibiting superior condensation performance because of its favorable thermophysical properties. The local heat transfer coefficient also increased with vapor quality up to approximately 0.95, after which the correlations showed different prediction trends, highlighting their varying treatment of high-quality condensation flow. The comparative analysis demonstrated that refrigerant thermal conductivity, latent heat of vaporization, viscosity, specific heat, and prandtl number significantly affect condensation performance. Overall, the study concludes that no single correlation accurately predicts condensation heat transfer under all operating conditions and refrigerant types.

***Keywords*—R-12, R-134a, R-409A, Refrigerants, Heat Transfer Correlations, Condensation Heat Transfer Coefficient, Condenser Performance and Thermal Analysis etc**

I. INTRODUCTION

Condensation heat transfer is a critical process in vapor compression refrigeration systems, as it directly influences condenser performance, system efficiency, and energy consumption. The selection of an appropriate refrigerant plays a significant role in determining the condensation heat transfer characteristics because refrigerants possess different thermo physical properties, such as thermal conductivity, viscosity, density, and latent heat of vaporization. R-134a has been widely used in refrigeration applications owing to its favorable thermodynamic performance, while R-409A has served as a retrofit refrigerant for replacing R-12 in medium- and low-temperature refrigeration systems.

Several empirical and semi-empirical condensation heat transfer correlations, including those proposed by Shah, Cavallini and Zecchin, Bohdal, Traviss, Huang, and Park, have been developed to predict condensation heat transfer coefficients under various operating conditions. However, the prediction accuracy of these correlations varies with refrigerant properties and flow conditions. Therefore, a comparative evaluation of R-134a and R-409A using these correlations is essential to understand their condensation heat transfer performance and suitability for refrigeration applications. This study evaluates the condensation heat transfer characteristics of R-134a and R-409A using widely accepted condensation heat transfer correlations under identical operating conditions. The analysis provides a comparative assessment of the refrigerants and examines the applicability of different correlations for condenser design and refrigeration system optimization..

A. Condensation Heat Transfer Coefficient

The local condensation heat transfer coefficient (h_{cond}) quantifies the effectiveness of heat transfer during a phase change. It is defined using Newton's Law of Cooling applied to the internal phase-change boundary layer:

$$h_{cond} = \frac{q}{T_{sat} - T_{wall}} \tag{1}$$

Where:

- h_{cond} = Local condensation heat transfer coefficient (W/m^2 · K)
- q = Local heat flux transferred through the tube wall (W/m^2)
- T_{sat} = Local saturation temperature of the condensing refrigerant (K)
- T_{wall} = Local temperature of the inner tube wall (K)

In the design and optimization of vapor compression refrigeration systems, h_{cond} is an essential parameter for several reasons.

Determining Thermal Resistance and Component Sizing
The overall heat transfer coefficient (U) of a condenser tube segment depends on the sum of its internal, conductive, and external thermal resistances:

$$\frac{1}{U \cdot A_o} = \frac{1}{h_{cond} \cdot A_i} + \frac{\ln(D_o/D_i)}{2\pi \cdot k_{wall} \cdot L} + \frac{1}{h_{ext} \cdot A_o} \tag{2}$$

Where A_i and A_o represent the internal and external surface areas, and h_{ext} is the external convective heat transfer coefficient (typically air or water-cooled). In air-cooled condensers, the air-side thermal resistance ($\frac{1}{h_{ext} \cdot A_o}$) is often high. Accurate knowledge of h_{cond} is required to prevent the internal thermal resistance from limiting performance, ensuring the heat exchanger is properly sized.
Impact on System Efficiency (COP)

A higher condensation heat transfer coefficient allows the condenser to reject its thermal load using a lower temperature difference ($\Delta T = T_{sat} - T_{wall}$). This enables the system to operate at a lower saturation condensing pressure (P_{cond}).

Lowering the condensing pressure reduces the pressure lift across the compressor, which decreases the required mechanical work input (W_{comp}) and increases the overall Coefficient of Performance ($\text{COP} = Q_{evap}/W_{comp}$) of the refrigeration system.

B. Advantages and Limitations of Existing Correlations

Table I: Comparison of correlation of different models

Correlation Model	Primary Target Flow Regime	Major Engineering Advantages	Documented Technical Limitations
Nusselt Model	Gravity-Dominated / Laminar Film	Simple analytical formulation; highly accurate at very low mass flux rates ($G <$ 50 kg/m^{2}s).	Fails at higher mass velocities because it ignores vapor shear and film turbulence; underpredicts h_{cond} in annular flow.
Shah Model	Shear-Dominated / Annular & Wavy	Broad empirical validation across diverse pipe diameters and refrigerant types; straightforward to implement.	Lacks explicit flow regime boundaries; shows higher prediction errors near critical pressures or in stratified flow regimes.
Cavallini & Zecchin	Shear-Dominated / Annular	Mathematically efficient; provides reliable predictions for pure HFC fluids operating at high mass velocities.	Poor accuracy in gravity-driven, stratified, or slug flow regimes; does not account for temperature glides in zeotropic mixtures.

C. Selection of Refrigerants

This study evaluates three distinct refrigerants that represent different stages in the evolution of working fluids: R-12, R-134a (an HFC replacement), and R-409A (a transitional HCFC blend).

- ***R-12 (Dichlorodifluoromethane, CF_2Cl_2)***
  R-12 is a synthetic halocarbon belonging to the Chlorofluorocarbon (CFC) family. Fordecades, it served as the global standard working fluid for domestic refrigerators, commercial water chillers, and automotive air conditioning systems. Thermo dynamically, R-12 features excellent performance characteristics, including low operating pressures, favorable transport properties, non-toxicity, and non-flammability. It is also fully miscible with inexpensive mineral oil lubricants. However, its high chemical stability allows it to persist in the environment for nearly a century, resulting in a high Ozone Depletion Potential ($\text{ODP} = 1.0$) and a high Global Warming Potential (GWP = 10,900).

- ***R-134a (1,1,1,2-Tetrafluoroethane, CH_2FCF_3)***
  R-134a is a Hydro fluorocarbon (HFC) that was introduced as the primary long-term substitute for R-12 in domestic and commercial applications. Because its molecular structure contains no chlorine atoms, its Ozone Depletion Potential is zero ($\text{ODP} = 0$).Thermodynamically, R-134a closely matches the volumetric cooling capacity and operating pressure profile of R-12, making it suitable for both new equipment and system retrofits. However, R-134a is completely immiscible with traditional mineral lubricants, requiring the use of synthetic Polyolester (POE) lubricants. These synthetic oils are highly hygroscopic, absorbing moisture quickly during system assembly and maintenance, which requires strict moisture controls. Additionally, R-134a carries a significant global warming potential (GWP = 1,430), making it subject to progressive phase-down regulations under the Kigali Amendment.

- ***R-409A (Commercial Designation: FX-56)***

R-409A is a zeotropic halocarbon blend composed of three constituent fluids: HCFC-22 (60%), HCFC-124 (25%), and HCFC-142b (15%). It was developed as a transitional "drop-in" service replacement for R-12 systems, allowing facility operators to replace the refrigerant without changing out traditional mineral oil or alkylbenzene lubricants. Because it is a zeotropic mixture, R-409A does not change phase at a single temperature; instead, it exhibits a temperature glide of approximately 8 K at condensing pressures. This means its boiling and condensing temperatures shift continuously across the heat exchanger as the constituent fluids change phase at different points. Furthermore, because it contains HCFC components, it retains a non-zero ozone depletion potential (ODP = 0.05) and a high global warming potential (GWP = 1,585). These environmental impacts have led to its phase-out alongside other ozone-depleting substances.

Table II: Compares the thermo physical properties of R-12, R-134a, and R-409A

Thermophysical Property Parameters	R-12 (CFC)	R-134a (HFC)	R-409A (HCFC Blend)
Molecular Weight (g/mol)	120.91	102.03	97.43
Normal Boiling Point at 1 atm (˚C)	-29.8	-26.1	-34.4 (Bubble) / -26.3 (Dew)
Saturation Condensing Pressure (MPa)	0.961	1.017	1.120
Latent Heat of Vaporization, Δh_{fg} (kJ/kg	132.4	163.0	185.2
Liquid Phase Density, ρ_l (kg/m^3)	1211.2	1146.7	1162.1
Vapor Phase Density, ρ_v (kg/m^3)	55.4	50.1	51.8
Liquid Thermal Conductivity, k_l (W/m · K)	0.066	0.076	0.071
Liquid Dynamic Viscosity, μ_l (μPa · s)	182.4	160.2	171.5

D. Research Motivation

The motivation driving this research stems from three interconnected factors:

- **Need for Evaluating Replacement Refrigerants** Environmental regulations require a continuous re-evaluation of working fluids in vapor compression systems. When transitioning away from an established fluid like R-12, engineers must find alternatives that match or exceed its thermal performance without increasing direct or indirect emissions. This requires detailed evaluations of thermodynamic cycles and transport properties to ensure new fluids can serve as efficient, long-term replacements.

- **Importance of Accurate Prediction of h_{cond}** The condensation heat transfer coefficient directly dictates the physical size, footprint, and manufacturing cost of condenser heat exchangers. If h_{cond} is underpredicted during design, the condenser will be oversized, leading to unnecessary material costs (copper and aluminum) and structural weight. Conversely, overpredicting h_{cond} results in an undersized condenser, forcing the system to operate at elevated head pressures, which degrades efficiency and accelerates compressor wear.

E. Research Objectives

- To address the challenges outlined in the problem statement, this study establishes the following primary objectives:
- Evaluate local and average condensation heat transfer coefficients (h_{cond}) for R-12, R-134a, and R-409A across a wide range of mass fluxes and vapor qualities.
- Conduct a comparative analysis of thermophysical properties to determine how changes in transport properties (such as liquid thermal conductivity and viscosity) impact heat transfer performance.
- Assess the predictive accuracy of existing heat transfer correlations (Nusselt, Shah, Cavallini & Zecchin, and Dobson & Chato) against baseline experimental and thermodynamic data.

.

II. LITERATURE REVIEW

Abhishek Kumar et al. (2026) conducted a thermodynamic assessment of several low-global-warming-potential (GWP) refrigerants (R-152a, R-515B, R-1234ze(E), R-1234yf, R-290, R-600a, R-600, and R-1270) as alternatives to R-134a in vapor compression refrigeration (VCR) systems. A steady-state simulation was performed under varying evaporator and condenser temperatures to evaluate the coefficient of performance (COP), compressor power, refrigerant mass flow rate, and volumetric cooling capacity. The results showed that R-600a, R-600, and R-152a achieved higher COP with lower compressor power than R-134a, while R-515B and R-1234ze(E) exhibited performance very close to the baseline refrigerant. Conversely, R-1234yf demonstrated lower energy efficiency and required greater compressor power. The study concluded that several low-GWP refrigerants can effectively replace R-134a when thermodynamic performance, compressor compatibility, and environmental impact are simultaneously considered [1].

Ariyadi et al. (2026) investigated the energy performance of R-32 and R-134a refrigerants for fisheries cold storage applications. The study compared refrigeration capacity, compressor power consumption, coefficient of performance (COP), and energy efficiency under practical operating conditions. Experimental analysis indicated that R-32 provided higher refrigeration capacity and improved energy efficiency due to its superior thermo physical properties, whereas R-134a demonstrated more stable operating characteristics. The authors concluded that R-32 represents a promising alternative for fisheries refrigeration systems because of its enhanced cooling performance and reduced energy consumption [2].

Chaturvedi et al. (2025) performed an energy analysis of a vapor compression refrigeration system employing R-134a, R-600a, and R-125. The study evaluated compressor work, energy destruction, COP, and second-law efficiency under different operating conditions. The results demonstrated that R-600a achieved the highest energy efficiency and lowest irreversibility, while R-134a maintained balanced thermodynamic performance. The authors emphasized that energy analysis provides an effective framework for selecting environmentally sustainable refrigerants with improved system efficiency [3].

Rayhan et al. (2025) compared the thermodynamic performance of refrigeration systems using R-134a, R-744 (CO_2), and R-32 for Indonesian fishing boats. Parameters including cooling capacity, compressor work, energy efficiency, and environmental impact were evaluated. The results showed that R-744 exhibited excellent environmental characteristics, whereas R-32 delivered superior energy efficiency under tropical operating conditions. The study recommended selecting refrigerants based on both climatic conditions and operational requirements for marine refrigeration applications [4].

Ajayi et al. (2024) developed a generalized condensation heat transfer coefficient and pressure drop model applicable over a wide range of reduced pressures. Experimental data covering various refrigerants and operating conditions were used to formulate and validate the proposed correlation. The model accurately predicted condensation heat transfer coefficients and pressure drops across different flow regimes while reducing prediction errors compared with conventional empirical correlations. The proposed model provides an improved tool for condenser design and refrigeration system optimization **[5]**.

Fang et al. (2024) proposed a new condensation heat transfer correlation based on flow pattern transitions for hydrocarbon refrigerants. Experimental investigations examined the influence of vapor quality, mass flux, and flow regimes on condensation performance. The developed correlation significantly improved prediction accuracy by incorporating flow pattern characteristics rather than relying solely on conventional dimensionless parameters. The study demonstrated that flow-regime-based models enhance the reliability of condenser performance prediction **[6]**.

Zhang et al. (2023) proposed a modified empirical correlation for condensation heat transfer in horizontal enhanced tubes using **R-32** and **R-410A** refrigerants. Experimental measurements were conducted under different operating conditions, including variations in mass flux, vapor quality, and condensation temperature. The modified correlation demonstrated improved prediction accuracy compared with existing models, particularly for enhanced tube geometries. The study concluded that incorporating surface enhancement effects substantially improves condensation heat transfer prediction **[7]**.

Table III. Comparison of different refrigerants for condensation

Ref. / Year / Author(s)	Refrigerant(s) Investigated	Methodology	Performance Parameters	Major Findings	Research Gap / Limitation
[1] (2026) Kumar et al.	R-152a, R-515B, R-1234ze(E), R-1234yf, R-290, R-600a, R-600, R-1270, R-134a	Steady-state thermodynamic simulation	COP, Compressor Power, Mass Flow Rate, Volumetric Cooling Capacity	R-600a, R-600, and R-152a achieved higher COP with lower compressor power; R-515B and R-1234ze(E) showed performance close to R-134a	Condensation heat transfer coefficients and pressure drop characteristics were not investigated.
[2] (2026) Ariyadi et al.	R-32, R-134a	Experiment al investigation	Cooling Capacity, Compressor Power, COP, Energy Efficiency	R-32 exhibited higher cooling capacity and better energy efficiency than R-134a	Limited to fisheries refrigeration; condensation performance was not analyzed.
[3] (2025) Chaturvedi et al.	R-134a, R-600a, R-125	Thermodyn amic and exergy analysis	COP, Compressor Work, Exergy Destruction, Second-law Efficiency	R-600a showed the highest exergy efficiency and lowest irreversibility	No experimental validation of condensation heat transfer.
[4] (2025) Rayhan et al.	R-134a, R-744, R-32	Thermodynami c analysis	Cooling Capacity, Compressor Work, COP, Environmental Impact	R-744 offered superior environmental performance, whereas R-32 achieved higher energy efficiency	Restricted to marine refrigeration applications.
[5] (2024) Ajayi et al.	Multiple Refrigerants	Experimental correlation development	Heat Transfer Coefficient, Pressure Drop	Proposed correlation improved prediction accuracy over a wide range of reduced pressures	System-level refrigeration performance was not evaluated.
[6] (2024) Fang et al.	Hydrocarbon Refrigerants	Experimental investigation	HTC, Vapor Quality, Mass Flux	Flow-pattern-based model significantly improved condensation prediction accuracy	Applicable mainly to hydrocarbon refrigerants.

III. PROPOSED METHOD

A. Thermodynamic properties correlations of Refrigerant R-12

Saturation pressure (kPa) -

$P = 3.08606081 \times 10^2 + 1.01429265 \times 10\ T_C + 1.25923916 \times 10^{-1} T_C^2 + 6.64737796 \times 10^{-4} T_C^3 + 8.78719702 \times 10^{-7} T_C^4 + 5.34706593 \times 10^{-10} T_C^5$

Specific volume of saturated liquid (m^3/kg) -
$v_l = (7.15891334 \times 10^{-1} + 1.65860646 \times 10^{-3} T_C + 7.65626021 \times 10^{-6} T_C^2 + 3.88996139 \times 10^{-8} T_C^3 + 1.79353924 \times 10^{-10} T_C^4 + 5.66482654 \times 10^{-12} T_C^5) \times 10^3$

Specific volume of saturated vapour (m^3/kg) -
$v_v = (5.53530732 \times 10 - 1.72114677 T_C + 3.34461227 \times 10^{-2} T_C^2 - 5.61572580 \times 10^{-4} T_C^3 + 7.21674933 \times 10^{-5} T_C^4 - 4.34119645 \times 10^{-8} T_C^5) \times 10^3$

Viscosity of saturated liquid (μPa-s) -
$\mu_l = 2.66803214 \times 10^2 - 2.43400566 T_C + 2.06007303 \times 10^{-2} T_C^2 - 1.58895252 \times 10^{-4} T_C^3 + 6.57636942 \times 10^{-7} T_C^4 - 1.39453493 \times 10^{-10} T_C^5$

Viscosity of saturated vapour (μPa-s) -
$\mu_v = 1.18008030 \times 10 + 4.26415275 \times 10^{-2} T_C - 2.55592946 \times 10^{-4} T_C^2 + 6.16247139 \times 10^{-6} T_C^3 + 4.64681816 \times 10^{-9} T_C^4 - 3.98438551 \times 10^{-11} T_C^5$

Specific heat of saturated liquid (kJ/kg/°K) -
$C_{Pl} = 9.25397369 \times 10^{-1} + 9.68941029 \times 10^{-4} T_C + 1.73127016 \times 10^{-5} T_C^2 + 5.70252532 \times 10^{-7} T_C^3 - 3.96317461 \times 10^{-10} T_C^4 + 6.74832862 \times 10^{-12} T_C^5$

Thermal conductivity of saturated liquid (mW/mK) -
$k_l = 7.58447928 \times 10 - 3.55418695 \times 10^{-1} T_C + 3.29146525 \times 10^{-4} T_C^2 -1.52328816 \times 10^{-6} T_C^3 + 1.37297011 \times 10^{-8} T_C^4 - 3.18151014 \times 10^{-10} T_C^5$

Surface tension of saturated liquid (mN/m) –
$\sigma_l = 1.17721372 \times 10 - 1.33499569 \times 10^{-1} T_C + 1.61916598 \times 10^{-4} T_C^2 + 3.53020876 \times 10^{-7} T_C^3 - 9.98044483 \times 10^{-10} T_C^4 + 4.19256139 \times 10^{-11} T_C^5$

B. Thermodynamic properties correlations of Refrigerant R-134a

Saturation pressure (kPa) -
$P = 2.93584534 \times 10^2 + 1.06079770 \times 10\ T_C + 1.47587926 \times 10^{-1} T_C^2 + 9.03309303 \times 10^{-4} T_C^3 + 1.63415795 \times 10^{-6} T_C^4 + 2.91966911 \times 10^{-9} T_C^5$

Specific volume of saturated liquid (m^3/kg) -
$v_l =(7.73075806 \times 10^{-1} + 1.95423748 \times 10^{-3} T_C + 9.89552192 \times 10^{-6} T_C^2 + 5.44339488 \times 10^{-8} T_C^3 + 4.09292135 \times 10^{-10} T_C^4 + 9.55479596 \times 10^{-12} T_C^5) \times 10^3$

Specific volume of saturated vapour (m^3/kg) -
$v_v = (6.92377156 \times 10 - 2.38272029 T_C + 5.06914555 \times 10^{-2} T_C^2 - 9.32599590 \times 10^{-4} T_C^3 + 1.27680175 \times 10^{-5} T_C^4 - 7.92203352 \times 10^{-8} T_C^5) \times 10^3$

Viscosity of saturated liquid (μPa-s) -
$\mu_l = 2.72952440 \times 10^2 - 3.41063726 T_C + 2.54699839 \times 10^{-2} T_C^2 - 2.92114697 \times 10^{-4} T_C^3 + 7.72746688 \times 10^{-6} T_C^4 - 7.91482029 \times 10^{-8} T_C^5$

Viscosity of saturated vapour (μPa-s) -
$\mu_v = 1.13280688 \times 10 + 2.67683004 \times 10^{-2} T_C + 5.23361575 \times 10^{-4} T_C^2 - 7.38501959 \times 10^{-6} T_C^3 + 1.35708342 \times 10^{-7} T_C^4 - 3.67119845 \times 10^{-10} T_C^5$

Specific heat of saturated liquid (kJ/kg/°K) -
$C_{Pl} = 1.34009929 + 3.02468424 \times 10^{-3} T_C + 1.22230142 \times 10^{-5} T_C^2 + 4.39681510 \times 10^{-7} T_C^3 - 6.87681771 \times 10^{-9} T_C^4 + 1.26351684 \times 10^{-10} T_C^5$

Thermal conductivity of saturated liquid (mW/mK) -
$k_l = 1.15597420 \times 10 - 1.44096983 \times 10^{-1} T_C + 4.03422136 \times 10^{-4} T_C^2 -3.39112495 \times 10^{-7} T_C^3 + 1.44110946 \times 10^{-9} T_C^4 - 2.76790349 \times 10^{-11} T_C^5$

Surface tension of saturated liquid (mN/m) –
$\sigma_l = 1.15597420 \times 10 - 1.44096983 \times 10^{-1} T_C + 1.85852254 \times 10^{-4} T_C^2 + 3.88558264 \times 10^{-7} T_C^3 + 2.24783451 \times 10^{-9} T_C^4 + 2.95599002 \times 10^{-11} T_C^5$

C. Thermodynamic properties correlations of Refrigerant R-409a

Saturation pressure (kPa) -
$P = 3.79534344 \times 10^2 + 1.25036610 \times 10\ T_C + 1.55289024 \times 10^{-1} T_C^2 + 8.07641807 \times 10^{-4} T_C^3 + 8.20454876 \times 10^{-7} T_C^4 - 9.14492630 \times 10^{-10} T_C^5$

Specific volume of saturated liquid (m^3/kg) -
$\rho_l = 1.29679997 \times 10^3 - 3.13742599 T_C - 6.56105745 \times 10^{-3} T_C^2 - 3.22737958 \times 10^{-5} T_C^3 - 1.17507550 \times 10^{-7} T_C^4 - 4.10382565 \times 10^{-9} T_C^5$

Specific volume of saturated vapour (m^3/ kg) -
$\rho_v = 1.67236725 \times 10 - 5.30555121 \times 10^{-1} T_C + 6.66465219 \times 10^{-3} T_C^2 - 4.25762184 \times 10^{-5} T_C^3 + 1.62523901 \times 10^{-7} T_C^4 - 2.82773743 \times 10^{-9} T_C^5$

Viscosity of saturated liquid (μPa-s) -
$\mu_l = 2.47340353 \times 10^2 - 2.77067445 T_C + 1.84402478 \times 10^{-2} T_C^2 - 1.39088074 \times 10^{-4} T_C^3 + 9.22767973 \times 10^{-7} T_C^4 - 4.33992707 \times 10^{-9} T_C^5$

Viscosity of saturated vapour (μPa-s) -
$\mu_v = 1.13875743 \times 10 + 4.16952891 \times 10^{-2} T_C - 5.26161617 \times 10^{-6} T_C^2 - 1.57160950 \times 10^{-6} T_C^3 - 1.24385859 \times 10^{-8} T_C^4 + 1.14298028 \times 10^{-9} T_C^5$

Specific heat of saturated liquid (kJ/kg/°K) -

$C_{Pl} = 1.15658972 + 2.35474133 \times 10^{-3}\, T_C + 1.70868344 \times 10^{-5}\, T_C^2 + 6.38364101 \times 10^{-8}\, T_C^3 + 5.59794649 \times 10^{-10}\, T_C^4 + 4.07855391 \times 10^{-11}\, T_C^5$

Thermal conductivity of saturated liquid (mW/mK) -
$k_l = 8.83009020 \times 10 - 4.18239199 \times 10^{-1}\, T_C + 2.74108127 \times 10^{-4}\, T_C^2 - 5.82054203 \times 10^{-7}\, T_C^3 - 6.45636948 \times 10^{-9}\, T_C^4 - 6.80520737 \times 10^{-11}\, T_C^5$

Surface tension of saturated liquid (mN/m) –
$\sigma_l = 1.30701982 \times 10 - 1.46424396 \times 10^{-1}\, T_C + 1.39961916 \times 10^{-4}\, T_C^2 + 3.58316129 \times 10^{-7}\, T_C^3 + 1.30709170 \times 10^{-9}\, T_C^4 + 2.29186543 \times 10^{-11}\, T_C^5$

Thermodynamic properties of refrigerants R-12, R-134a and R-409a is calculated by putting value of saturation temperature from -30˚C to 60˚C with interval of 2˚C in JAVA SCRIPT programming of above equations. Then we get Table.1, Table.2 and Table.3 which shows the thermo dynamic properties of refrigerants R-12, R-134a and R-409a. Thermodynamic properties correlations of R-12 have a maximum MAPE 0.2237198% and minimum MAPE 0.0015322%. Thermodynamic properties correlations of R-134a have a maximum MAPE 0.3816663% and minimum MAPE 0.0113188%. Thermodynamic properties correlations of R-409a have a maximum MAPE 0.0905326% and minimum MAPE 0.0001967%.

IV. VALIDATION AND ANALYSIS

A. Local heat transfer coefficient of R12, R134a and R409a using different correlation

Local and average heat transfer coefficient for R-12, R-134a and R-409a at 45 ˚C condensing temperature is calculated by using programming of six correlations. The calculated heat transfer coefficients of three refrigerants are compared with each other. Comparison is presented either as a absolute value of heat transfer coefficient or as a ratio of heat transfer coefficient. The comparison is performed for average and local heat transfer coefficients.

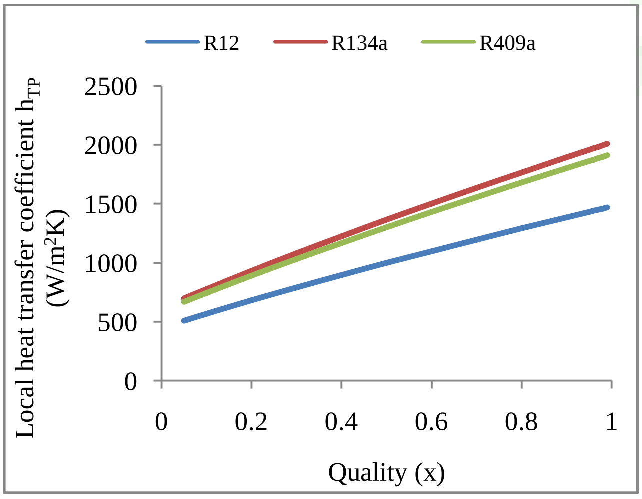

Fig.1 Local heat transfer coefficient of R12, R134a and R409a from Cavallini and Zecchin correlation at condensing temperature 45˚C

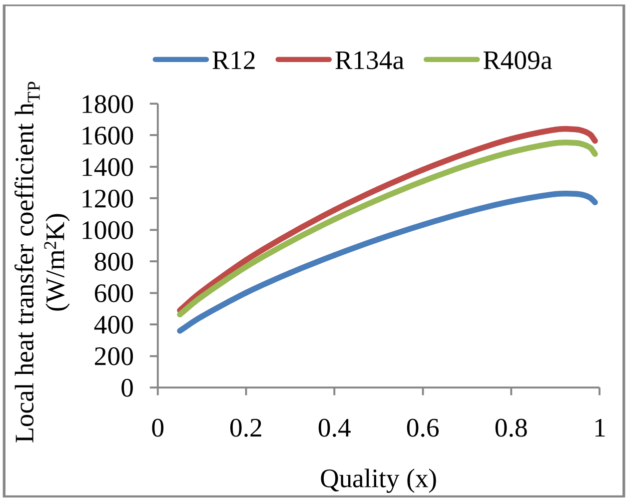

Fig.2: Local heat transfer coefficient of R12, R134a and R409a from Shah correlation at condensing temperature 45˚C

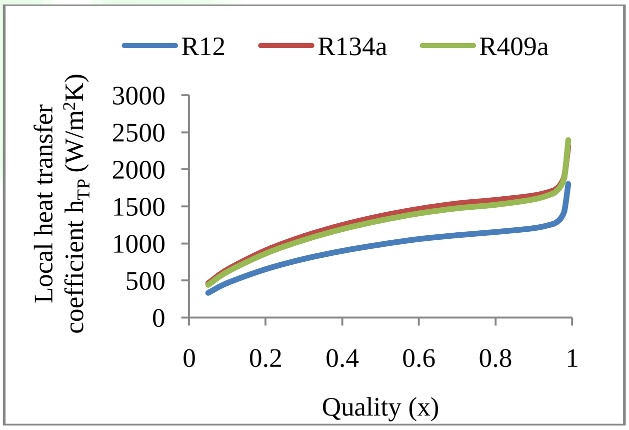

Fig.3: Local heat transfer coefficient of R12, R134a and R409a from Traviss et al correlation at condensing temperature 45˚C

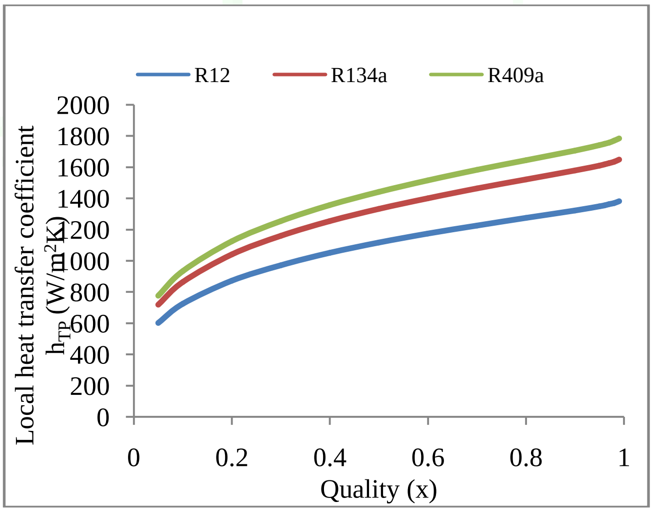

Fig. 4: Local heat transfer coefficient of R12, R134a and R409a from Bohdal correlation at condensing temperature 45˚C

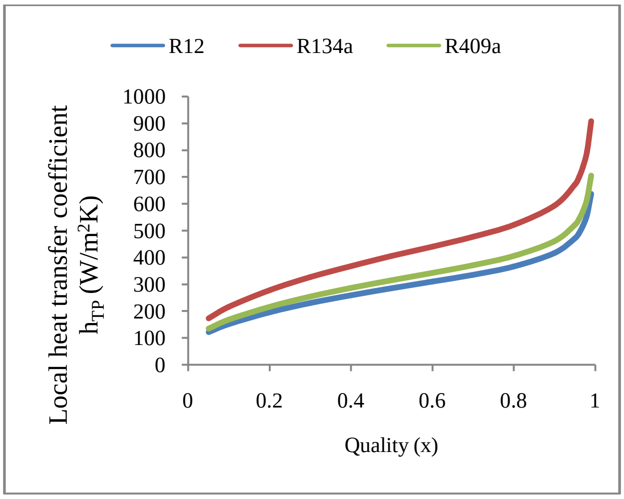

Fig.5 Local heat transfer coefficient of R12, R134a and R409a from Park correlation at condensing temperature 45˚C

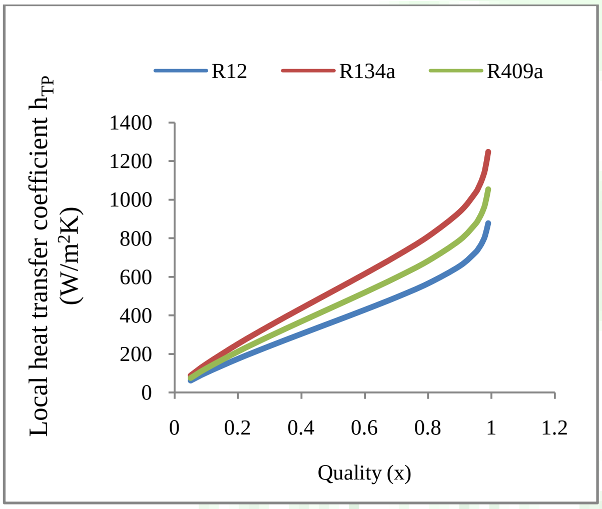

Fig.6 Local heat transfer coefficient of R12, R134a and R409a from Huang correlation at condensing temperature 45˚C

Figure 1, 2, 3, 4, 5, and 6 shows the local heat transfer coefficient of R12, R134a and R409a using Cavallini and Zecchin, Shah, Traviss, Bohdal, Park and Huang correlation at condensing temperature 45˚C. Cavallini and Zecchin, Shah, Traviss, Park and Huang correlation shows the local heat transfer coefficient of R134a is higher than R409a and R12 while Bohdal correlation shows the local heat transfer coefficient of R409a is higher than R134a and R12 higher mass flux. As the quality increases local heat transfer coefficient also increases upto 0.95, after 0.95 quality behaviour of local heat transfer coefficient change for the three refrigerants. Cavallini and Zecchin correlation shows the linear increment, Shah correlation shows sudden decrement while Traviss, Bohdal, Park and Huang correlation shows sudden increament in local heat transfer coefficient for three refrigerant after 0.95 quality.

B. Comparison of correlations

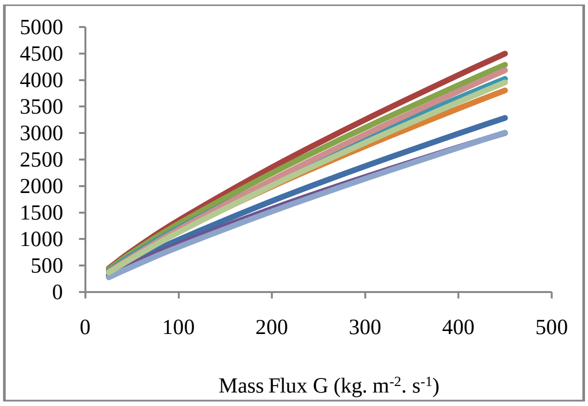

Fig. 7 Average heat transfer coefficient for R-12, R-134a and R-409a at condensing temperature 45 ˚C

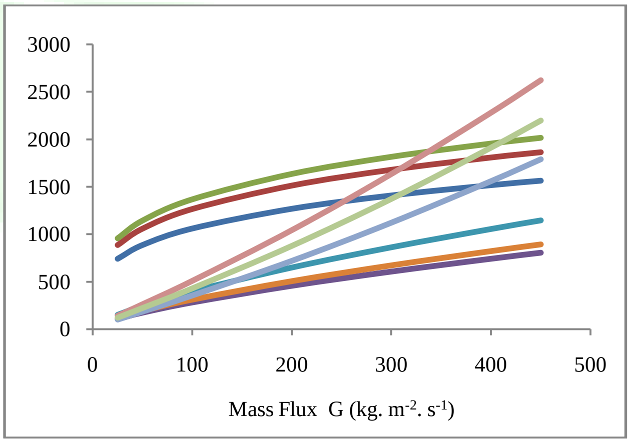

Fig. 8 Average heat transfer coefficient for R-12, R-134a and R-409a at condensing temperature 45 ˚C

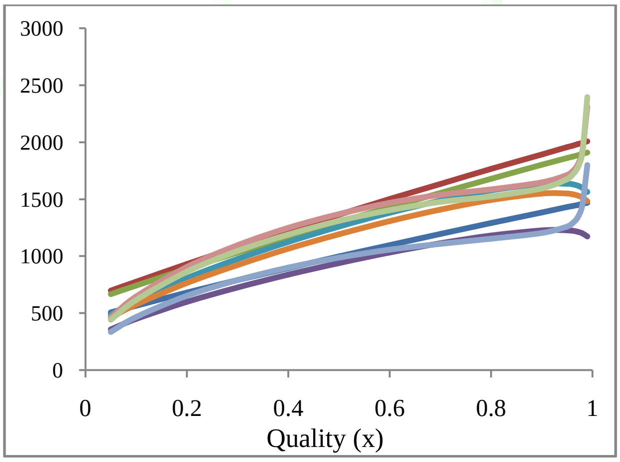

Fig. 9 Local heat transfer coefficient for R-12, R-134a and R-409a at condensing temperature 45 ˚C

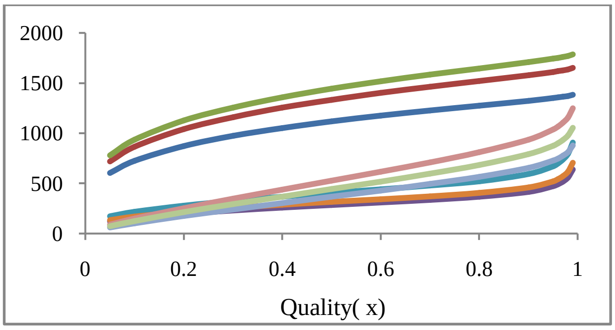

Fig. 10 Local heat transfer coefficient for R-12, R-134a and R-409a at condensing temperature 45 ˚C

Figures 7 to 10 present a comparative analysis of the average and local condensation heat transfer coefficients of R-12, R-134a, and R-409A predicted using the Cavallini and Zecchin, Shah, Traviss, Bohdal, Park, and Huang correlations at a condensing temperature of 45°C. The results indicate that the predicted heat transfer coefficients vary considerably depending on the selected correlation and refrigerant. For the average heat transfer coefficient, the Cavallini and Zecchin correlation consistently predicts higher values than the Shah correlation, with increases of approximately 9.49% for R-12, 11.9% for R-134a, and 12.5% for R-409A, while the Traviss correlation provides values comparable to or slightly higher than Shah, particularly at higher mass fluxes. Similarly, among the Bohdal, Huang, and Park correlations, the Huang correlation predicts the highest average heat transfer coefficients, whereas the Park correlation consistently gives the lowest values. At higher mass fluxes, Huang predicts average heat transfer coefficients that are 14.6%, 40.6%, and 9.04% higher than Bohdal for R-12, R-134a, and R-409A, respectively, while Bohdal predicts values significantly higher than Park. A similar trend is observed for the local heat transfer coefficient at a mass flux of 100 kg m^{-2} s^{-1}, where both Cavallini and Zecchin and Traviss correlations predict substantially higher values than the Shah correlation, particularly at higher vapor qualities. Likewise, the Bohdal and Huang correlations consistently predict considerably higher local heat transfer coefficients than the Park correlation for all three refrigerants. Overall, the analysis demonstrates that condensation heat transfer predictions are highly dependent on the selected correlation, with Cavallini and Zecchin and Huang generally yielding the highest predictions, whereas the Park correlation provides the most conservative estimates. These variations highlight the significant influence of correlation formulation on the prediction of condensation heat transfer performance and emphasize the importance of selecting an appropriate correlation for accurate condenser design and refrigeration system analysis.

V. Conclusion

The comparative analysis of R-12, R-134a, and R-409A shows that the predicted condensation heat transfer coefficients are highly dependent on the selected correlation. The average heat transfer coefficient increases with increasing mass flux, while the local heat transfer coefficient increases with vapor quality for all refrigerants. Among the evaluated models, the Cavallini and Zecchin and Huang correlations generally predict higher heat transfer coefficients, whereas the Park correlation provides the lowest predictions. Overall, R-134a exhibits better condensation heat transfer performance than R-12 and R-409A under most operating conditions, indicating its suitability for efficient refrigeration applications. The results emphasize the importance of selecting an appropriate condensation heat transfer correlation for accurate condenser design and performance evaluation..

References

[1]. Camilleri Tamrat, Bimrew, Dessie Tarekegn, and Velmurugan Paramasivam. "Numerical and experimental analysis of the effectiveness of solar air heaters combined with a continuous V-shaped ribbed roughness parameter." *International Journal of Thermo fluids* (**2026**): 101652.

[2]. Singh, Jitendra, Jaigopal Ambade, and Atul Lanjewar. "Thermal–hydraulic evaluation of solar air heaters with symmetrical gap arc rib roughness." *Journal of Thermal Analysis and Calorimetry* 150, no. 18 (**2025**): 14183-14201.

[3]. Singh, Rohit, and Ramadas Narayanan. "Comprehensive Review of Thermal and Thermo hydraulic Performance in Solar Air Heaters with Advanced Artificial Roughness Geometries." *Energies* 18, no. 23 (**2025**): 6157.

[4]. Alam, Tabish, and Deepak Gupta. "Thermo hydraulic performance of hybrid ribs pattern combining V and arc shape ribs in solar air heater." *Experimental Heat Transfer* 37, no. 7 (**2024**): 1084-1099.

[5]. Singh, Jitendra, and Atul Lanjewar. "Thermal performance of solar air heater having discrete symmetrical arc rib with staggered rib roughness." *Proceedings of the Institution of Mechanical Engineers, Part C: Journal of Mechanical Engineering Science* 238, no. 2 (**2024**): 598-617.

[6]. Rajendran, Vijayakumar, Muthuraman Ponrajan Vikram, Sung Chul Kim, Paride Gullo, Abdullah Alodhayb, Saravanan Pandiaraj, and Rajendran Prabakaran. "Enhancing the performance of a solar air heater by employing the broken V-shaped ribs. " *Environmental Science and Pollution Research* 30, no. 31 (**2023**): 77807-77818.

[7]. Dubey, Manoj Kumar, and Om Prakash. "Enhanced Heat Transfer Performance in a Solar Air Heater using discrete V-Rib Geometry with Gap." Research Square (**2023**).

[8]. Kumar, Rahul, Sujit Kumar Verma, Naveen Kumar Gupta, Andrés Z. Mendiburu, Abhishek Sharma, Tabish Alam, and Sayed M. Eldin. "Experimental assessment and modelling of solar air heater with V shape roughness on absorber plate." *Case Studies in Thermal Engineering* 43 (**2023**): 102784.

[9]. Rajendran, Vijayakumar, Harichandran Ramasubbu, Jaya Venkatesh Rajarathinam, and Ramanan Pichandi. "Experimental study on the thermal performance of a solar air heater integrated with multi-geometry arrangements over the absorber plate." *Environmental Science and Pollution Research* 29, no. 25 (**2022**): 38331-38345.

[10]. Rajendran, Vijayakumar, Harichandran Ramasubbu, Jaya Venkatesh Rajarathinam, and Ramanan Pichandi. "Experimental study on the thermal performance of a solar air heater integrated with multi-geometry arrangements over the absorber plate." *Environmental Science and Pollution Research* 29, no. 25 (**2022**): 38331-38345.

[11]. Rajendran, Vijayakumar, Harichandran Ramasubbu, Jaya Venkatesh Rajarathinam, and Ramanan Pichandi. "Experimental study on the thermal performance of a solar air heater integrated with multi-geometry arrangements over the absorber plate." *Environmental Science and Pollution Research* 29, no. 25 (**2022**): 38331-38345.

[12]. Alam, Tabish, Chandan Swaroop Meena, Nagesh Babu Balam, Ashok Kumar, and Raffaello Cozzolino. "Thermo-hydraulic performance characteristics and optimization of protrusion rib roughness in solar air heater." *Energies* 14, no. 11 (**2021**): 3159.

[13]. Kazemi Moghadam, Hamid, Seyed Soheil Mousavi Ajarostaghi, and Sébastien Poncet. "Numerical modelling of an innovative arc shape rib based solar air heater." *Proceedings of the Institution of Mechanical Engineers, Part C: Journal of Mechanical Engineering Science* 235, no. 24 (**2021**): 7992-8012.

[14]. Wang, Dengjia, et al. "Evaluation of the performance of an improved solar air heater with “S” shaped ribs with gap."Solar Energy 195 **(2020**): 89-101.

[15]. Saravanakumar, P. T., D. Somasundaram, and M. M. Matheswaran. "Thermal and thermo-hydraulic analysis of arc shaped rib roughened solar air heater integrated with fins and baffles."Solar Energy 180 **(2019**): 360-371.

[16]. Kumar, Rajesh, and Prabha Chand. "Performance prediction of extended surface absorber solar air collector with twisted tape inserts." Solar Energy 169 (**2018): ** 40-48.

[17]. Aboghrara, Alsanossi M., et al. "Performance analysis of solar air heater with jet impingement on corrugated absorber plate."Case studies in thermal engineering 10 **(2017):** 111-120

[18]. Rajesh Maithani, J.S. Saini, “Heat transfer and friction factor correlations for a solar air heater duct roughened artificially with V-ribs with symmetrical gaps” Experimental Thermal and Fluid Science, Volume70, Pages 220-227, **2016**.

[19]. Ehsan Ebrahimnia-Bajestan, Mohammad Charjouei Moghadam, Hamid Niazmand, Weerapun Daungthongsuk, Somchai Wongwises, “Experimental and numerical investigation of nano-fluids heat transfer characteristics for application in solar heat exchangers”, International Journal of Heat and Mass Transfer, Volume 92, Pages 1041–1052, **2016.**

[20]. Hamdi E. Ahmed, M.I. Ahmed, M.Z. Yusoff, M.N.A. Hawlader, Habeeb Al-Ani “Experimental study of heat transfer augmentation in non-circular duct using combined nano-fluids and vortex generator” International Journal of Heat and Mass Transfer, Volume 90, Pages 1197–1206, **2015**

[21]. Alireza Zamani Aghaie, Asghar B. Rahimi, Alireza Akbarzadeh “A general optimized geometry of angled ribs for enhancing the thermo-hydraulic behavior of a solar air heater channel - A Taguchi approach” Elsevier Renewable Energy, Volume 83, Pages 47-54, **2015.**

[22]. Adem Acır, Ismail Ata “A study of heat transfer enhancement in a new solar air heater having circular type tabulators” *Elsevier Journal of the Energy Institute*, Pages 1-11, **2015.**

[23]. Anil Kumar, Man-Hoe Kim “Effect of roughness width ratios in discrete multi V-rib with staggered rib roughness on overall thermal performance of solar air channel” *Elsevier Solar Energy*, Volume 119, Pages 399–414, **2015.**

[24]. Dongxu Jin, Manman Zhang, Ping Wang, Shasha Xu, “Numerical investigation of heat transfer and fluid flow in a solar airheater duct with multi V-shaped ribs on the absorber plate” *Elsevier Energy*, Volume 89, Page 178-190, **2015.**

[25]. Chao Ma, Xiaoling Chen, Jianfei Wang, Shusheng Zang, Yongbin Ji, “An experimental investigation of heat transfer characteristics for steam cooling and air cooling in a rectangular channel roughened with parallel ribs” *Experimental Thermal and Fluid Science*, Volume 64, Page 142–151, **2015.**

